AUTHOR QUERY FORM

ELSEVIER	**Journal: SAA** **Article Number: 13648**	**Please e-mail your responses and any corrections to:** **E-mail: corrections.esch@elsevier.sps.co.in**

Dear Author,

Please check your proof carefully and mark all corrections at the appropriate place in the proof (e.g., by using on-screen annotation in the PDF file) or compile them in a separate list. Note: if you opt to annotate the file with software other than Adobe Reader then please also highlight the appropriate place in the PDF file. To ensure fast publication of your paper please return your corrections within 48 hours.

For correction or revision of any artwork, please consult http://www.elsevier.com/artworkinstructions.

Any queries or remarks that have arisen during the processing of your manuscript are listed below and highlighted by flags in the proof. Click on the 'Q' link to go to the location in the proof.

Location in article	Query / Remark: click on the Q link to go Please insert your reply or correction at the corresponding line in the proof
Q1	Your article is registered as a regular item and is being processed for inclusion in a regular issue of the journal. If this is NOT correct and your article belongs to a Special Issue/Collection please contact e.mohan@elsevier.com immediately prior to returning your corrections.
Q2	Please confirm that given name(s) and surname(s) have been identified correctly.
Q3	This section comprises reference that occur in the reference list but not in the body of the text. Please position each reference in the text or, alternatively, delete it. Any reference not dealt with will be retained in this section.

Please check this box if you have no corrections to make to the PDF file ☐

Thank you for your assistance.

Spectrochimica Acta Part A: Molecular and Biomolecular Spectroscopy xxx (2015) xxx–xxx

Contents lists available at ScienceDirect

Spectrochimica Acta Part A: Molecular and Biomolecular Spectroscopy

journal homepage: www.elsevier.com/locate/saa

Vibrational studies (FTIR and Raman), conformational analysis, NBO, HOMO–LUMO and reactivity descriptors of S-methyl thiobutanoate, $CH_3CH_2CH_2C(O)SCH_3$

Diego M. Gil, María Eugenia Tuttolomondo, Aída Ben Altabef*,[1]

INQUINOA – CONICET – UNT, Instituto de Química Física, Facultad de Bioquímica, Química y Farmacia, Universidad Nacional de Tucumán, San Lorenzo 456, T4000CAN Tucumán, Argentina

HIGHLIGHTS

- The molecular structure of S-methyl thiobutanoate was determined by ab-initio and DFT calculations.
- The experimental and theoretical results confirm the presence of two stable conformations.
- The infrared and Raman spectra were recorded and the bands observed were assigned to the vibrational normal modes.
- Global and local reactivity descriptors were computed to predict reactivity.

GRAPHICAL ABSTRACT

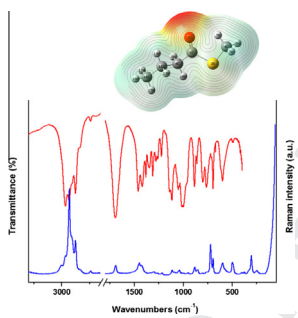

ARTICLE INFO

Article history:
Received 12 November 2014
Received in revised form 9 March 2015
Accepted 22 April 2015
Available online xxxx

Keywords:
S-methyl thiobutanoate
DFT calculations
Internal barrier to rotation
Infrared and Raman spectroscopy
Global and local descriptors

ABSTRACT

In the present article, the molecular structure of S-methyl thiobutanoate, $CH_3CH_2CH_2C(O)SCH_3$ was determined by ab initio (MP2) and DFT calculations using different basis sets. The infrared and Raman spectra for the liquid phase were also recorded and the bands observed were assigned to the vibrational normal modes. The experimental and calculations confirm the presence of two most stable conformers, one with *pseudo anti–syn* conformation and another with *gauche–syn* conformation. The study was completed using natural bond orbital (NBO) and AIM analysis. The molecular properties like dipole moment, molecular electrostatic potential surface (MEP) and HOMO–LUMO molecular orbitals were calculated to get a better insight of the properties of the title molecule. Global and local reactivity descriptors were computed in order to predict reactivity and reactive sites on the molecule for nucleophilic, electrophilic and radical attacks.

Introduction

Thioesters, compounds with general formula RCOSR', are an obligatory intermediate in many key biosynthetic reactions, including the formation and degradation of fatty acids and complex lipids, and the regeneration and dehydration of adenosine triphosphate [1,2]. They also participate in the synthesis of a large number of cellular components such as peptides, sterols, and others. In addition, thioesters also play an important role in protein tagging with ubiquitin, which tags the protein for degradation [1].

The structural and conformational properties of thioesters are of great interest because of their close relation to many biomolecules where they constitute their most important property because these molecules must adopt definite forms to carry out specific biological functions. For example, coenzyme A plays an important role in metabolic energy production and is recognized as a

* Corresponding author. Tel.: +54 381 4311044; fax: +54 381 4248169.
E-mail address: altabef@fbqf.unt.edu.ar (A. Ben Altabef).
[1] Member of the Research Career of CONICET, Argentina.

http://dx.doi.org/10.1016/j.saa.2015.04.097
1386-1425/© 2015 Published by Elsevier B.V.

universal carrier of activated acyle groups. The HS-CoA reacts with acyle groups to form RCO-SCoA acylcoenzyme A which is due to the high reactivity of thioesters in nucleophilic acyl transfer reactions as compared with oxoesters. S-methyl thioesters with an acyl chain length of 2-10 carbons are of great interest because of their very powerful odors often associated with cheese flavor and their low perception thresholds [3]. S-methyl thioacetate is quantitatively the most important in cheeses. Previous studies suggested that S-methyl thioesters were probably produced through a reaction involving methanethiol and acyl-CoAs during cheese ripening. This process is produced by different bacteria like *Brevibacterium antiquum*, *Brevibacterium aurantiacum* and *Brevibacterium linens* [3].

The conformational study of several methyl thioesters has been reported by different groups [4–7]. The general tendency found in these compounds indicates that the *syn* conformation (C=O double bond *syn* with respect to S–CH_3 single bond) prevails over the *anti* one. A microwave study for S-methyl thioformate demonstrated that this molecule exists only in the *syn* conformation [6].

The compound S-methyl thiobutanoate, $CH_3CH_2CH_2C(O)SCH_3$, is commercially available, but its molecular structure has not been studied. Our group have studied various esters with the general formula CF_3CO_2R (R = –CH_3, –CH_2CH_3, –CH_2CF_3) [8–10] including the related thioester, $CF_3COSCH_2CH_3$ [11].

In this article, we have performed a conformational analysis to determine the most stable conformation of the title compound. Infrared and Raman spectra were recorded in liquid phase and these experimental measurements were complemented by quantum chemical calculations to obtain an optimized molecular structure and a scaled quantum mechanical force field. The spectral features were assigned to the different normal modes of vibration. The conformational study was complemented by natural bond orbital (NBO) analysis to assess the significance of hyper-conjugative interactions which would favor one conformation over another and the study of the reactivity was performed by AIM approach. HOMO–LUMO analysis was performed to determine some molecular properties like ionization potential, electron affinity, electronegativity, chemical potential, hardness, softness and global electrophilicity index. Local reactivity descriptors were calculated to identify the preferred sites for electrophilic, nucleophilic and radical attacks.

Experimental

Samples of $CH_3CH_2CH_2C(O)SCH_3$ for spectroscopy measurements were purchased from Sigma–Aldrich and used without further purification. The purity of S-methyl thiobutanoate was checked by FTIR spectra.

Infrared and Raman spectroscopy

Infrared spectra for $CH_3CH_2CH_2C(O)SCH_3$ in the liquid phase were recorded in the 4000–400 cm^{-1} range at room temperature (RT) using a Perkin-Elmer GX1 Fourier transform infrared instrument. The Raman spectrum of the liquid at RT between 3500 and 50 cm^{-1} was measured on a Thermoscientific DXR Smart Raman instrument. Data were collected using a diode-pump, solid-state laser of 780 nm (5 cm^{-1} spectral resolution). A confocal aperture of 25 μm pinhole was used. In order to achieve a sufficient signal to noise, 100 expositions of 2 s were accumulated for the sample. The laser power was maintained at 5 mW when collecting data.

Computational methods

Calculations were performed using the resources of the United Kingdom National Service for Computational Chemistry Software (NSCCS), running the Gaussian 03 suite of programs [12]. Geometry optimizations were performed at the MP2 [13] and DFT levels using a variety of basis sets. Electron correlation was then considered using the MP2 approach with the 6-311G(d,p), 6-311++G(d,p) and 6-311++G(3df,3pd) basis set [14–17]. DFT calculations were performed using Becke's three-parameter hybrid exchange functional [18] (B3) combined with both the Lee–Yang–Parr gradient-corrected correlation functional [19] (LYP) and the same basis sets as for the MP2 calculations. The second DFT method used, mPW1PW91 [20] applies a modified Perdew–Wang exchange functional and Perdew–Wang 91 correlation functional [20]. All calculations were performed using standard gradient techniques and default convergence criteria.

The potential energies associated with the SCCC, CCCC and CSCC dihedral angles were calculated at MP2, B3LYP and mPW1PW91 levels using the 6-311++G(d,p) basis sets, with that torsional angle frozen and all other parameters allowed to relax. The total energy curves were prepared in steps of 10° using default convergence criteria as implemented in the Gaussian program.

A natural bond orbital (NBO) calculation was performed at the B3LYP/6-311++G(d,p) level using the program NBO 3.1 [21] as implemented in the Gaussian 03 package. This analysis was performed to understand various second order interactions between the filled orbitals of one subsystem and the vacant orbitals of another in order to have a measure of intra-molecular delocalization of hyper-conjugation. In addition, reactivity was analyzed with Bader's atoms in molecules theory (AIM) by using the AIM2000 code [22,23].

Molecular properties such as ionization potential (IP), electron affinity (EA), electronegativity (χ), chemical potential (μ), hardness (η), softness (s) and global electrophilicity index (ω) were deduced from HOMO–LUMO analysis employing B3LYP/6-311++G(d,p) level.

Raman activities (SRa) calculated with the Gaussian 03 program were converted to relative Raman intensities (IRa) using the following relationship derived from the intensity theory of Raman scattering [24]:

$$I_i = \frac{f(\nu_0 - \nu_i)^4 S_i}{\nu_i[1 - \exp(-hc\nu_i/kT)]} \quad (1)$$

where ν_0 is the laser exciting wavenumber in cm^{-1} (in this work, we used the excitation wavenumber ν_0 = 12820.5 cm^{-1}, which corresponds to the wavelength of 780 nm of the solid state laser), ν_i is the vibrational wavenumber of the *i*th normal mode (cm^{-1}) and S_i is the Raman scattering activity of the normal mode ν_i. f (it is a constant equal to 10^{-12}). This is a suitably chosen common scaling factor for all peak intensities.

Results and discussion

Quantum chemical calculations

Conformational analysis

The potential energy scans around the SCCC, CSCC and CCCC dihedral angles calculated at B3LYP/6-311++G(d,p) level are shown in Fig. 1(a–c), respectively. Total energies (E), differences in total energies (ΔE), free energies (G) and differences in free energies for the possible conformations found for $CH_3CH_2CH_2C(O)SCH_3$ calculated at B3LYP/6-311++G(d,p) approximation are presented in Table 1. Fig. 2 shows the possible conformations predicted for the title compound. When the SCCC dihedral angle was varied (Fig. 1(a)), conformers I and II were observed. Conformer I shows an *anti–syn* orientation (CCCC dihedral angle is 180° and *syn* between the C=O double bond and the C–S single bond) and conformer II shows a *pseudo anti–syn* orientation (CCCC dihedral angle

Please cite this article in press as: D.M. Gil et al., Vibrational studies (FTIR and Raman), conformational analysis, NBO, HOMO–LUMO and reactivity descriptors of S-methyl thiobutanoate, $CH_3CH_2CH_2C(O)SCH_3$, Spectrochimica Acta Part A: Molecular and Biomolecular Spectroscopy (2015), http://dx.doi.org/10.1016/j.saa.2015.04.097

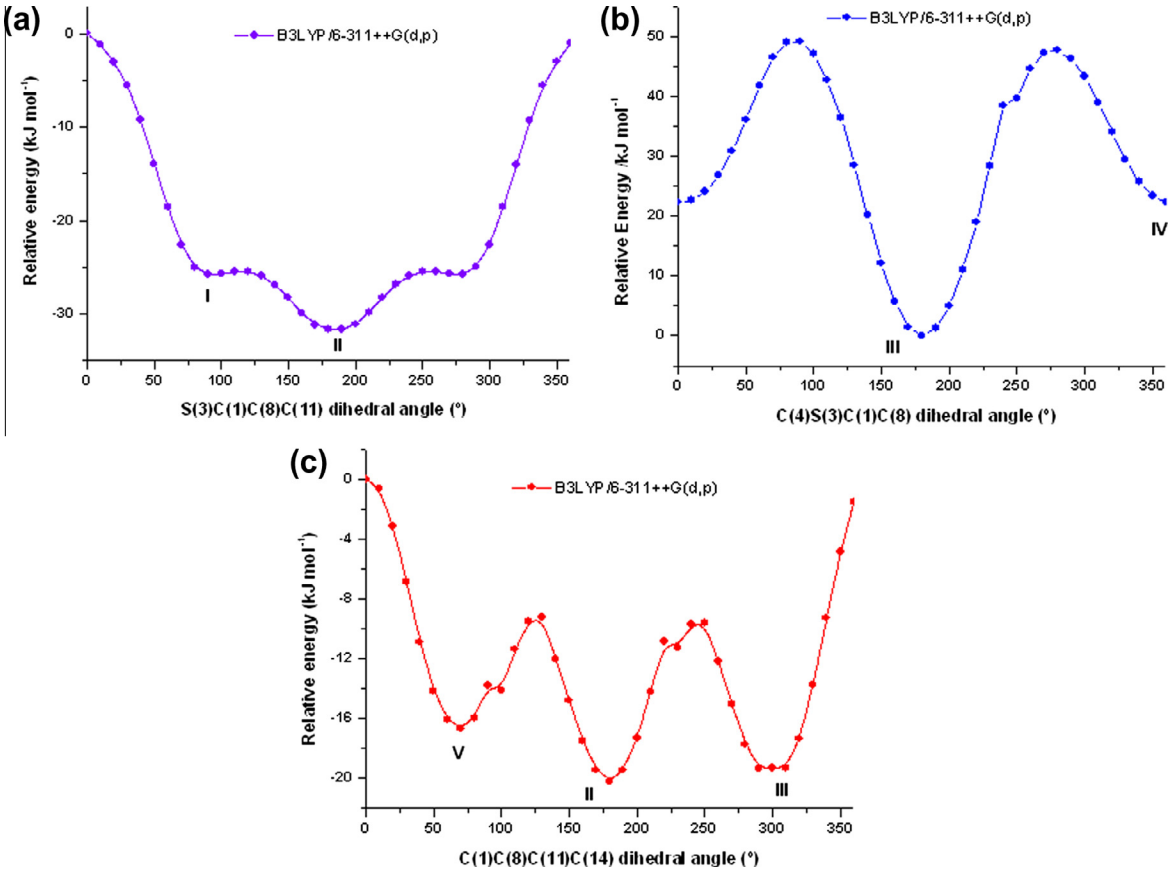

Fig. 1. Potential energy curves for $CH_3CH_2CH_2C(O)SCH_3$ as a function of the (a) S(3)–C(1)–C(8)–C(11), (b) C(4)–S(3)–C(1)–C(8) and (c) C(1)–C(8)–C(11)–C(14) dihedral angles calculated at B3LYP/6-311++G(d,p) approximation.

Table 1
Total energies (E), differences in total energies (ΔE), free energies (G) and differences in free energies for the possible conformations of $CH_3CH_2CH_2C(O)SCH_3$ calculated at B3LYP/6-311++G(d,p) approximation.

	I	II	III	IV	V
E^a	−670.091318	−670.091770	−670.091488	−670.083934	−670.082235
G^a	−669.983842	−669.985837	−669.985636	−669.976532	−669.974477
ΔE^b	1.19	0	0.75	20.55	25.00
ΔG^b	5.23	0	0.53	24.40	29.79

[a] Absolute energies in Hartrees.
[b] Relative energies in kJ mol^{-1}; $\Delta E = E$(conformer) − E(II); $\Delta G = G$(conformer) − G(II).

is 177° and *syn* between the C=O double bond and the C–S single bond). The differences in total energy between the two minima is 5.23 kJ mol^{-1} calculated at B3LYP/6-311++G(d,p) approximation indicating that conformers II is more stable. When we varied the CSCC dihedral angle (Fig. 1(b)), two additional minima were observed, namely III and IV. Conformer III presents a *gauche–syn* orientation (CCCC dihedral angle is 68° and *syn* between the C=O double bond and the C–S single bond) and the orientation observed for conformer IV was *gauche–anti* (CCCC dihedral angle is 68° and *anti* between the C=O double bond and the C–S single bond). The difference in total energy between both conformers is high (20 kJ mol^{-1}) indicating that only conformer III could be observed in experimental data (see below). The scans corresponding to the variation of CCCC dihedral angle (Fig. 1(c)) shows three minima, two for conformers II and III and a third conformation namely V. Conformer V presents a *gauche–anti* conformation (*gauche* between C(8)–C(11) and *anti* between the C=O double bond and the C–S single bond). There was an important difference in total energy between the three conformations indicating that conformers II and III were more stable than conformer V.

All the minima observed in the curves were optimized. From these calculations, the free energy values for each conformer could be obtained. Table 1 summarizes the values of free energies and the differences of free energies relative to the conformer II that was predicted to be the most stable conformer. For conformers II and III, the free energy calculated using the B3LYP/6-311++G(d,p) approximation was used along with the average temperature of the experiment to estimate the population of each conformer that should be observed in gas phase. As the difference in free energy was calculated to be 0.53 kJ mol^{-1} (conformer II lower in energy), the ratio of II to III conformers was predicted to be 0.45:0.59.

Molecular structure

Taking into account the high flexibility of this compound and the several possible conformations, most of which were undetectable at room temperature, full optimizations of the two lowest energy conformers on the potential energy surface of the title compound were carried out using the B3LYP/6-311++G(d,p) approximation. The calculated structural parameters for conformers II and III of the title compound are given in Table 2. The calculated

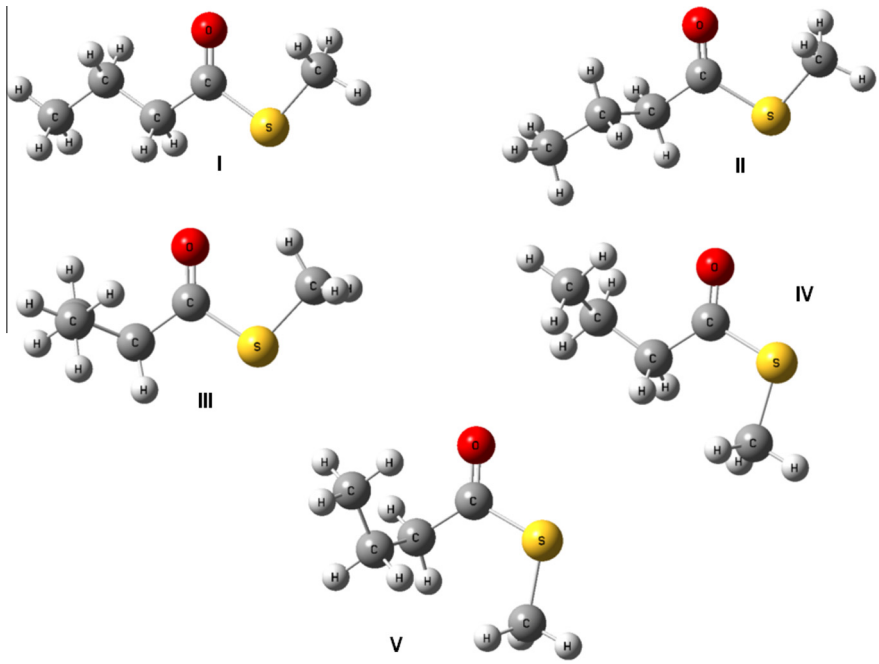

Fig. 2. Molecular structure for the conformers of $CH_3CH_2CH_2C(O)SCH_3$. The complete description is presented in the body of the text.

geometrical parameters were compared with those experimental values reported for related compounds [4,11].

Conformer II was predicted to be the most stable form (Fig. 2). It exhibits a C(1)–C(8)–C(11)–C(14) torsion angle of 177° and the CH_3 group was on the same side of the carbonyl group. In this structure, one of the methyl C–H bonds coexists in the plane of the ester group. Fig. S1 shows the optimized molecular structure of the *pseudo anti–syn* conformer of the title compound calculated at B3LYP/6-311++G(d,p) level. According to the Della Védova et al., the *syn* form for the $CH_3C(O)SCH_3$ is more stable than the *anti* one. This affirmation was supported by gas electron diffraction (GED) measurements [4].

The geometrical parameters calculated at the B3LYP and MP2 levels of approximations using 6-311++G(3df,3pd) basis sets for conformers I, II and III of the title compound are shown in Table S1. The theoretical description of molecules containing C–S bonds requires the use of highly polarized basis functions. As was found for different molecules containing C–S bonds such as $CH_3SO_2SCH_3$ [25] and $CF_3C(O)SCH_2CH_3$ [11], the inclusion of extra polarization functions (beyond a single d-function) is necessary to predict the bond distances in these molecules accurately. The most sensitive parameter to this orbital description was the C–S bond length, which was shortened 0.012 Å at B3LYP when we replaced the 6-311++G(d,p) basis sets with 6-311++G(3df,3pd) basis sets. All bonds involving the sulfur atom were shortened, but the remaining bond lengths were relatively unchanged. This produced a calculated geometry close to the experimental structure determined by GED measurements [4,11]. The MP2/6-311++G(3df,3pd) level of theory estimates matches well all the bond distances and angles reported using GED data for related molecules [4,11]. The longer bond length observed at the B3LYP method is due to the over-estimation of electron–electron repulsions.

Table 2
Selected calculated and experimental (taken from relative compounds) structural parameters of the two lowest energy conformers of $CH_3CH_2CH_2C(O)SCH_3$.

Parameter[a]	II	III	Experimental
Bond distances (Å)			
C–H (mean)	1.093	1.093	1.092[b]
C(4)–S(3)	1.824	1.825	1.805[b]
S(3)–C(1)	1.804	1.804	1.781[b]
C(1)=O(2)	1.206	1.206	1.216[c]
C(1)–C(8)	1.517	1.521	1.546[c]
C(8)–C(11)	1.538	1.536	1.533[c]
C(11)–C(14)	1.530	1.531	1.533[c]
Angles (°)			
C(1)–S(3)–C(4)	101.1	101.0	99.20[b]
S(3)–C(1)=O(2)	123.4	123.2	122.8[b]
O(2)=C(1)–C(8)	123.7	123.9	123.4[b]
C(1)–C(8)–C(11)	111.7	113.0	–
C(8)–C(11)–C(14)	112.4	113.4	–
Dihedral angles (°)			
C(4)–S(3)–C(1)–C(8)	179.5	176.5	–
S(3)–C(1)–C(8)–C(11)	120.4	139.6	–
C(1)–C(8)–C(11)–C(14)	177.1	68.8	–

[a] Calculated at the B3LYP/6-311++G(d,p) level of approximation. See Figure S1 for atoms numbering.
[b] Taken from Ref. [4].
[c] Taken from Ref. [11].

Internal barrier decomposition schemes

The study of the nature of the barrier to rotation of the C(1)–S and C(1)–C (sp^2) bonds in terms of hyper-conjugative, steric and electrostatic interactions will give us an insight into the reasons for the relative stability of conformers III and IV. The potential-energy surface for the target torsion angle was calculated in 10° steps in the range 0–180°, allowing all other geometrical parameters to relax. The energy profiles were fitted to a sixth-order Fourier expansion:

$$V(\theta) = \sum_{i=1}^{6} \frac{1}{2} V_{iN} (1 - \cos\ iN\theta) \quad (2)$$

where N, the symmetry number, equals 1. No contributions to torsional energies from zero-point energy were taken into account.

The decomposition of the total energy function and the analysis of the different V_i terms has previously been shown to be an effective method of analyzing the stabilization of different conformations in molecular systems [8–11,26]. The six V_i terms calculated

for the title compound using the B3LYP/6-311++G(d,p) basis sets are shown in Table S2. Fig. 3 shows the Fourier decomposition of the total energy function calculated at the same level of theory. With their large values, V_1 and V_2 are the main contributions to the rotational barrier, with $V_2 > V_1 > V_3$. The terms V_{4-6} are less significant when deconvoluting the potential-energy curve. The magnitudes and signs of the two main terms are similar regardless of the level of theory used to calculate them. V_2 is usually associated with conjugative and hyper-conjugative effects that have a periodicity of 180°. As for V_1, it usually accounts for interactions between local dipoles and for steric interactions. The V_3 term is associated with unfavorable bond-bond eclipsing interactions, exhibiting a three-fold periodicity for a torsion involving sp^3-hybridized sulfur atoms. Fig. 3(a) shows that the barrier between the *syn* and *anti* forms is approximately 24 kJ mol^{-1}. It can be seen that the highest value corresponds to the V_2 parameter, but this contributes equally to the two forms. The values of both V_1 and V_3 are the determinants for the stability of the *syn* form. Both parameters are dependent by electrostatic interactions. This is further supported by the value of the dipole moment for the *syn* form (1.15 D) that is much smaller than the *anti* form (4.21 D). Fig. 3(b) shows that the barrier between the *pseudo anti–syn* and *gauche–syn* forms is approximately 10 kJ/mol. The large V_3 and V_1 values are the main contributions to the rotational barrier, while $V_2 > V_5 > V_4 > V_6$ are less significant when deconvoluting the potential energy curve. The V_3 term is large and negative, showing that there is a strong preference for the *pseudo anti–syn* and *gauche–syn* form over the *anti–syn* form. The V_3 term is associated with unfavorable bond-bond eclipsing interactions between the CH_2 groups, exhibiting a 3-fold periodicity for a torsion involving sp^3-hybridized carbon atoms while the behavior of the V_1 term is less favorable for both transition states. The balance between the V_3 and V_1 terms contributed to the stabilization of the *pseudo anti–syn* form. The absolute values of V_3 and V_1 gave the barrier energy and form respectively.

NBO analysis

Natural bond orbital (NBO) analysis is a useful tool for understanding delocalization of electron density from occupied Lewis-type (donor) NBOs to properly unoccupied non-Lewis type (acceptor) NBOs within the molecule. The stabilization of orbital interaction is proportional to the energy difference between the interacting orbitals. Therefore, the interaction having strongest stabilization takes place between effective donors and effective acceptors. The interaction between bonding and anti-bonding molecular orbitals can be quantitatively described in terms of the NBO approach that is expressed by means of second-order perturbation interaction energy $E(2)$. This energy represents the estimate of the off-diagonal NBO Fock matrix element. The stabilization energy $E(2)$ associated with i (donor) → j (acceptor) delocalization is estimated from the second-order perturbation approach as given below:

$$E(2) = E_{ij} = q_i \frac{F^2(i,j)}{\varepsilon_j - \varepsilon_i} \quad (3)$$

where q_i is the donor orbital occupancy, ε_i and ε_j are diagonal elements (orbital energies) and $F(i,j)$ is the off-diagonal Fock matrix element.

The role of hyper-conjugative interactions in the stabilization of the conformations observed for the title compound has been studied using NBO analysis, where the hyper-conjugation represents the transfer of an electron between a lone pair or bonding orbital and an anti-bonding orbital. Table 3 shows the main hyper-conjugative interactions for the *anti–syn* (conformer I), *pseudo anti–syn* (conformer II) and *gauche–syn* (conformer III) of S-methyl thiobutanoate. In terms of the NBO analysis, the hyper-conjugative interactions are more favored in the *pseudo anti–syn* conformation than the others. Thus, lone pairs of the oxygen and sulfur atoms transfer electronic charge to the anti-bonding σ^* orbital of the C–S and C=O bonds and these stabilizing interactions are stronger for the *pseudo anti–syn* form. For a larger anomeric effect lpσ S(3) → σ^* C(1)–O(2) a C–S bond strengthening is expected. As seen in Table 3, this interaction for the *pseudo anti–syn* conformer is higher than for the *gauche–syn* form. This is reflected in the higher value of the stretching frequency of the C(O)–S bond for the *pseudo anti–syn* conformer (703 cm^{-1}) with respect to the *gauche–syn* (697 cm^{-1}). A comparative study of the skeleton internal barrier and the corresponding NBO analysis for this family of compounds was performed by the authors and will be the subject of another paper to be published. The values of occupation and energy of the different natural bond orbitals are shown in Table S3.

AIM analysis

The quantum theory of atoms in molecules has been useful in the characterization of bonds through a topological analysis of the electronic charge density and their Laplacian at the bond critical point (BCP) [22]. In the AIM theory the nature of the bonding interaction can be determined through an analysis of the properties of the charge density, ρ, and its Laplacian $\nabla^2(\rho)$ at the BCP, and through the properties of the atoms, which are obtained by integrating the charge density over the atom orbitals [22]. The molecular graph for the *pseudo anti–syn* and *gauche–syn* conformers of the title compound using the AIM program calculated at B3LYP/6-311++G(d,p) level is presented in Fig. S2. Table S4 shows the bond critical point data for S-methyl thiobutanoate molecule. As seen in Table S4, the values of charge density for the C(1)–O(2), C(1)–S(3), S(3)–C(4) and C(1)–C(8) bond critical points of both conformations are relatively high and the $\nabla^2(\rho)$ is negative. These results indicate that the charge density has been concentrated in the inter-nuclear region.

The AIM methodology self-consistently partitioned any system and its properties into its atomic fragments, considering the gradient vector field of its electron density distribution. Koch et al. have proposed criteria based on the AIM theory to establish hydrogen bonding; the electron density at the BCP and its Laplacian are the most representative for this kind of interaction [28]. However, the energy density at the bond critical point (H_{BCP}) has proved to be a more sensible and appropriate index than $\nabla^2(\rho)$ to characterize the nature of hydrogen bonds [29].

The results obtained for electron density (ρ_{BCP}), its Laplacian ($\nabla^2(\rho)_{BCP}$), electron kinetic energy density (G_{BCP}), electron potential energy density (V_{BCP}) and total electron energy density (H_{BCP}) at the bond critical points (BCPs) for *pseudo anti–syn* and *gauche–syn* conformers of the title compound evaluated by means of the AIM approach at the B3LYP/6-311++G(d,p) level are presented in Table S5. The values of electron density at the BCP are in agreement with the values range reported by Koch and Popelier (0.002–0.004). Rozas et al. have suggested criteria that can be used to characterize hydrogen bonds (HB) [29]. Weak HB interactions show both $\nabla^2(\rho)_{BCP}$ and $H_{BCP} > 0$, and medium HB interactions show $\nabla^2(\rho)_{BCP} > 0$ and $H_{BCP} < 0$, while strong HB interactions show both $\nabla^2(\rho)_{BCP}$ and $H_{BCP} < 0$. According to the values reported in Table S5, all $\nabla^2(\rho)_{BCP}$ and H_{BCP} parameters for both conformers were greater than zero indicating that O(2)···H(7) hydrogen bonds are weak interactions.

The ellipticity (ε) at the BCP is a sensitive index to monitor the π-character of bond. The ε is related to λ_1 and λ_2, which correspond to the eigen values of the Hessian and is defined by the relationship: $\varepsilon = (\lambda_1/\lambda_2) - 1$. The ellipticity values for bonds C(1)–O(2)

Please cite this article in press as: D.M. Gil et al., Vibrational studies (FTIR and Raman), conformational analysis, NBO, HOMO–LUMO and reactivity descriptors of S-methyl thiobutanoate, $CH_3CH_2CH_2C(O)SCH_3$, Spectrochimica Acta Part A: Molecular and Biomolecular Spectroscopy (2015), http://dx.doi.org/10.1016/j.saa.2015.04.097

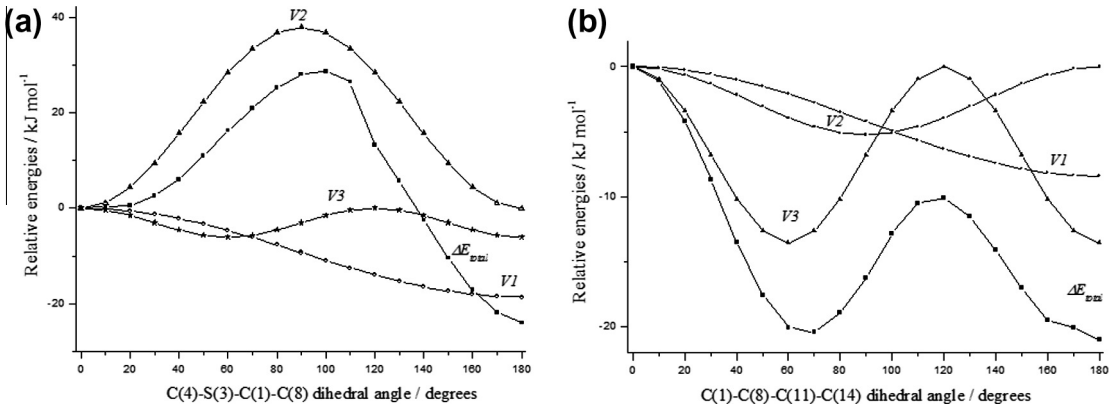

Fig. 3. Fourier decomposition of the potential function V(θ) for $CH_3CH_2CH_2C(O)SCH_3$ for the CSCC and CCCC dihedral angles calculated at B3LYP/6-311++G(d,p) level.

Table 3
Relevant hyper-conjugative interactions in kJ mol^{-1} for $CH_3CH_2CH_2C(O)SCH_3$ calculated at the B3LYP/6-311++G(d,p) level.

Interactions (donor → acceptor)[a]	Anti–syn (I)	*Pseudo anti – syn* (II)	Gauche–syn (III)
lpσ O(2) → σ* C(1)–S(3)	5.98	7.11	6.94
lpσ O(2) → σ* C(1)–C(8)	10.62	10.12	10.37
lpπ O(2) → σ* C(1)–S(3)	147.34	146.72	145.84
lpπ O(2) → σ* C(1)–C(8)	72.44	69.89	71.48
lpσ O(2) → σ* C(4)–H(7)	2.26	3.89	3.55
lpσ S(3) → σ* C(1)–O(2)	20.02	22.32	22.49
lpσ S(3) → σ* C(1)–O(2)	125.27	128.87	126.15
Total	383.93	388.92	386.82

[a] lp denotes a lone pair of σ or π orbital on the specified atom.

and C(1)–S(3) were 0.0329 and 0.2350, respectively for the *pseudo anti–syn* conformer. The ε values for the *gauche–syn* conformer corresponding to these bonds were 0.0313 and 0.2329. The lower values of the ellipticity index confirm that there is electron delocalization through the corresponding atoms. However, the higher ellipticity values for C(1)–S(3) indicate that the electrons of these bonds are not delocalized [22].

Molecular electrostatic potential (MEP)

The molecular electrostatic potential surface (MEP) was determined by B3LYP/6-311++G (d,p) level in order to understand the relative polarity of the molecule. The MEP (electrostatic potential mapped onto an electron iso-density surface) may be used to predict reactive sites for electrophilic attack (electron rich region) and nucleophilic attack (electron poor region). Even when the two molecules are structurally very similar, MEPs make clear that this similarity is not carried over into their electrophilic/nucleophilic reactivates. The MEP surface simultaneously displays molecular size, shape and electrostatic potential in terms of color grading and is a very useful tool in the investigation of correlation between molecular structure and the physicochemical property relationship of molecules including biomolecules and drugs [30–32]. The red and blue region refers to the electron rich and electron poor region while the slightly electron rich region is indicated by yellow and the green region in MEPs suggests an almost neutral region. The variation in electrostatic potential produced by a molecule is largely responsible for the binding of a drug to its receptor binding sites, as the binding site in general is expected to have opposite areas of electrostatic potential. The MEPs map and contour plot of the *pseudo anti–syn* conformer of S-methyl thiobutanoate generated at optimized geometry of the title molecule using the GaussView 05 software is shown in Fig. 4. It is evident from the MEPs map that the region around the hydrogen atoms of the carbon atoms is electron deficient (light blue color), therefore binding site for electrophiles. The region around the oxygen atom corresponding to the C=O group represents the most electron rich region and it is the binding site for nucleophiles. As seen in Fig. 4, the region around the sulfur atom is slightly electron rich.

HOMO–LUMO analysis

The energy gap between the highest occupied and the lowest unoccupied molecular orbital is an important quantum chemical parameter that determines molecular electrical transport properties and is a measure of electron conductivity. The HOMO energy characterizes electron ability to give while the LUMO energy characterizes electron ability to accept, and the gap between the HOMO and LUMO molecular orbital characterizes the chemical reactivity and kinetic stability of the molecule. A molecule with a small energy gap is more polarizable and is generally associated with a high chemical reactivity, low kinetic stability and is also termed as a soft molecule [33]. The HOMO and LUMO plot for the title compound with the corresponding energies and energy gap is presented in Fig. 5. The HOMO of the title molecule (−7.0736 eV) is located in the sulfur atom, the oxygen of the C=O group and in the methyl group bound to the S atom. The LUMO (−0.8416 eV) is spread over the entire molecule. The high value of the energy gap between HOMO–LUMO indicates that the molecule shows high chemical stability and low reactivity. Table S6 shows the band gap of the *anti* and *gauche* conformers of some thioesters such as $CF_3C(O)SCH_2CH_3$, $CH_3C(O)SCH_2CH_3$ and for the most stable conformers of the title compound. As can be seen in Table S6, the gap band between the HOMO and LUMO frontier molecular orbitals is higher in the thioesters where the carbonyl group is bound to an alkyl group (methyl or propyl), but the lowest gap band value is observed in the compound bound to the CF_3 group. It indicates that the $CF_3C(O)SCH_2CH_3$ in both conformations is more reactive and more stable than $CH_3C(O)SCH_2CH_3$ and $CH_3CH_2CH_2C(O)SCH_3$.

Global and local reactivity descriptors

The global reactivity descriptors like chemical potential, electronegativity, hardness, softness and global electrophilicity index can be calculated using DFT methods. Following Parr and Pearson [34], the electronic chemical potential describing the escaping tendency of the electron from a stable system can be calculated as:

$$\mu = -\frac{(I+A)}{2} \quad (4)$$

where I = ionization potential and A = electron affinity. Electronegativity (χ) is described as the negative of the electronic chemical potential. Chemical hardness (η) demonstrates the resistance to alteration in electron distribution and is well correlated

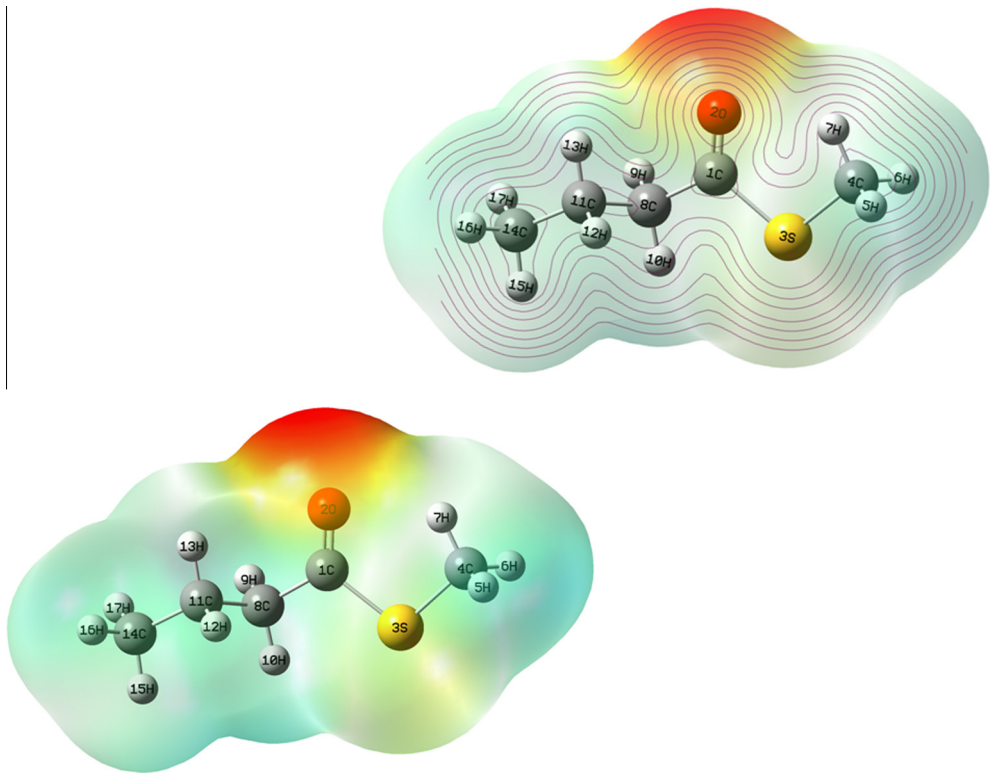

Fig. 4. MEP surface and contour plots for $CH_3CH_2CH_2C(O)SCH_3$ calculated at B3LYP/6-311++G(d,p) level.

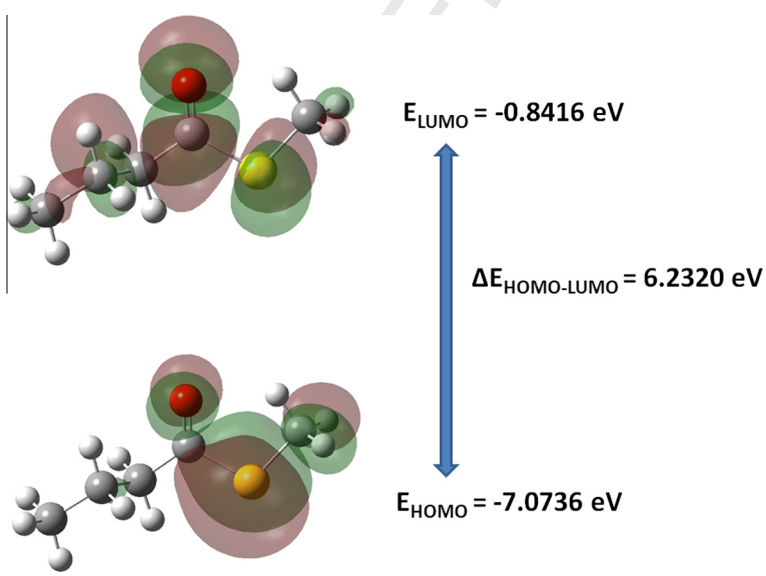

Fig. 5. HOMO and LUMO plots for $CH_3CH_2CH_2C(O)SCH_3$ calculated at B3LYP/6-311++G(d,p) level with the corresponding energies and band gap.

with the stability and reactivity of the chemical system. Hardness is expressed by the following equation:

$$\eta = \frac{I - A}{2} \tag{5}$$

The inverse of hardness is expressed as global softness:

$$s = \frac{1}{2\eta} \tag{6}$$

The global electrophilicity index (ω), introduced by Parr et al. [34] is calculated in terms of chemical potential and hardness:

$$\omega = \frac{\mu^2}{2\eta} \tag{7}$$

This value assesses energy decreasing due to maximal electron flow between donor and acceptor. The calculated values of the global reactivity descriptors for the title molecule are collected in Table 4. The value of chemical hardness is 3.1160 eV. In terms of chemical hardness, if a molecule has a large HOMO–LUMO gap, it is hard. Conversely, if the HOMO–LUMO gap is small, it is soft. One can also relate molecular stability to hardness, which means that the molecule with smaller HOMO–LUMO gap is more reactive.

Please cite this article in press as: D.M. Gil et al., Vibrational studies (FTIR and Raman), conformational analysis, NBO, HOMO–LUMO and reactivity descriptors of S-methyl thiobutanoate, $CH_3CH_2CH_2C(O)SCH_3$, Spectrochimica Acta Part A: Molecular and Biomolecular Spectroscopy (2015), http://dx.doi.org/10.1016/j.saa.2015.04.097

The local reactivity descriptor like the Fukui function indicates the preferred regions where a chemical species (molecule) will amend its density when the electron number is modified or indicates the tendency of the electron density to deform at a given position upon accepting or donating electrons [35]. The condensed or atomic Fukui functions on the *k*th atom site, for electrophilic (f_k^-), nucleophilic (f_k^+) and free radical (f_k^0) attacks are defined as:

$$f_k^+ = [q(N+1) - q(N)] \text{ for nucleophilic attack} \quad (8)$$

$$f_k^- = [q(N) - q(N-1)] \text{ for electrophilic attack} \quad (9)$$

$$f_k^0 = \frac{1}{2}[q(N+1) - q(N-1)] \; forradicalattack \quad (10)$$

where q_k is the atomic charge (Mulliken, NBO, etc.) at the *k*th atomic site in the anionic ($N+1$), cationic ($N-1$) or neutral molecule. According to Parr and Yang [35], the sites in chemical species with the largest of Fukui function (f_k) values show high reactivity for corresponding attacks. The Fukui functions (FF) were calculated using the program proposed by Chamarro et al. [36] The FF values for the title compound calculated at B3LYP/6-311++G(d,p) level are shown in Table 5 and Fig. S3. The FF (f_k^+, f_k^-, f_k^0), local softness (S_k^+, S_k^-, S_k^0) and electrophilic indices (ω_k^+, ω_k^-, ω_k^0) of the individual atoms of $CH_3CH_2CH_2C(O)SCH_3$ are presented in Table S7. The highest f_k^+ value was predicted for the C(1) atom indicating that it is the preferred site for nucleophilic attack. According to the values reported in Table 4, the reactivity order for nucleophilic attack is C(1) > O(2) > S(3). The electrophilic reactivity order is: S(3) > O(2) while the order of sites for free radical attack is: S(3) > C(1) > O(2). Local softness (S_k^+, S_k^-, S_k^0) and electrophilic indices (ω_k^+, ω_k^-, ω_k^0) are calculated using the following equations [37]:

$$S_k^+ = Sf_k^+, \quad S_k^- = Sf_k^-; \quad S_k^0 = Sf_k^0 \quad (11)$$

$$\omega_k^+ = \omega f_k^+, \quad \omega_k^- = \omega f_k^-; \quad \omega_k^0 = \omega f_k^0 \quad (12)$$

where +, − and 0 signs show nucleophilic, electrophilic and radical attacks, respectively. These equations predict the most electrophilic site in a system with the maximum value of S_k^+ and ω_k^+ while maximum value of S_k^- and ω_k^- corresponds to the nucleophilic site in the molecule. According to the values of local softness and local electrophilic indices reported in Table S7, the reactivity order for nucleophilic attack is identical to f_k^+, f_k^- and f_k^0.

Vibrational analysis

The assignment of the experimental IR and Raman bands to the normal modes of vibration of $CH_3CH_2CH_2C(O)SCH_3$ was based on the comparison of related molecules [11,38,39] and assisted by the theoretical calculations performed in this work with different levels of theory. DFT calculations reproduced the normal wavenumbers of vibrations with the following root-mean-square deviations (RMSD) for each basis set: 65 cm^{-1} for 6-31G(d), 56 cm^{-1} for 6-311G(d,p) and 53 cm^{-1} for 6-311++G(d,p). The results with the combination B3LYP/6-311++G(d,p) were used for the vibrational analysis to facilitate the comparison of the present results with those obtained previously for related molecules [11,38,39]. At room temperature, most bands are attributable to the same fundamental for *pseudo anti–syn* and *gauche–syn* conformations. The IR and Raman spectra of the liquid substance demonstrate the presence of both conformers of the title compound by resolution of several fundamental modes of vibration. The FTIR and Raman spectra of the liquid substance are shown in Fig. 6. The wavenumbers of the observed spectra and the approximate description of modes of both conformers of the title compound are given in Table 6.

Table 4
Global reactivity descriptors data for $CH_3CH_2CH_2C(O)SCH_3$ calculated at B3LYP/6-311++G(d,p) level.

Ionization potential, *I* (eV)	7.0736
Electron affinity, *A* (eV)	0.8416
Electronegativity, χ (eV)	3.9576
Chemical potential, μ (eV)	−3.9576
Chemical hardness, η (eV)	3.1160
Global softness, *s* (eV^{-1})	0.1605
Global electrophilicity index, ω (eV)	2.5132

Table 5
Values of Fukui functions for S-methyl thiobutanoate.[a]

Atoms[b]	*f*(−)	*f*(+)	*f*(0)
C(1)	0.0136	0.5421	0.2778
O(2)	0.1151	0.2664	0.1908
S(3)	0.7961	0.0900	0.4430
C(4)	0.0212	0.0020	0.0116
H(5)	0.0219	0.0020	0.0120
H(6)	0.0240	0.0022	0.0131
H(7)	0.0001	0.0001	0.0001
C(8)	0.0028	0.0199	0.0113
H(9)	0.0024	0.0515	0.0269
H(10)	0.0002	0.0049	0.0026
C(11)	0.0016	0.0088	0.0052
H(12)	0.0008	0.0055	0.0032
H(13)	0.0000	−0.0001	0.0000
C(14)	0.0000	0.0028	0.0014
H(15)	0.0000	0.0002	0.0001
H(16)	0.0000	0.0002	0.0001
H(17)	0.0001	0.0013	0.0007

[a] Calculated at B3LYP/6-311++G(d,p) level.
[b] See Fig. 4 for atoms numbering.

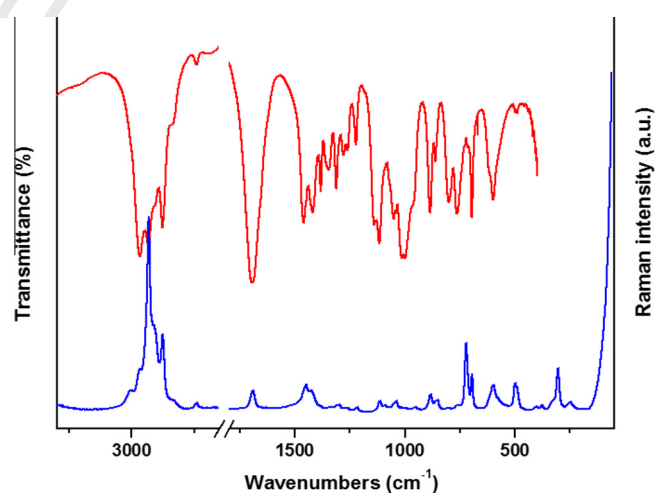

Fig. 6. Experimental IR and Raman spectra of $CH_3CH_2CH_2C(O)SCH_3$ in liquid phase.

Assignment of bands

Methyl and methylene group modes. The shoulder observed at 2984 cm^{-1} in the Raman spectrum is assigned to the anti-symmetric stretching mode of the CH_3 group bound to the S atom. The band corresponding to the CH_3 symmetric stretching mode appears as a shoulder at 2948 cm^{-1} in the Raman spectrum. The band located at 2840 cm^{-1} in the IR spectrum (2915 cm^{-1} in Raman) is assigned to the symmetric stretching mode of the methyl bound to the CH_2 group.

The bands located at 1463 and 1458 cm^{-1} in the IR spectrum are assigned to the $CH_3(CH_2)$ anti-symmetric bending mode. The weak band located at 1425 cm^{-1} in the IR spectrum (1430 and 1422 cm^{-1} in Raman) is assigned to the $CH_3(S)$ anti-symmetric

Please cite this article in press as: D.M. Gil et al., Vibrational studies (FTIR and Raman), conformational analysis, NBO, HOMO–LUMO and reactivity descriptors of S-methyl thiobutanoate, $CH_3CH_2CH_2C(O)SCH_3$, Spectrochimica Acta Part A: Molecular and Biomolecular Spectroscopy (2015), http://dx.doi.org/10.1016/j.saa.2015.04.097

Table 6
Observed bands in the IR and Raman spectra of $CH_3CH_2CH_2C(O)SCH_3$. Calculated wavenumbers, IR and Raman intensities for *gauche–syn* and *pseudo anti–syn* conformers of the title molecule and their tentative assignments.

Experimental		Calculated[c]						Approximate description of mode[d]
Infrared[a]	Raman[b]	Syn, pseudo anti	IR int.	Raman int.	Syn, gauche	IR int.	Raman int.	
Liquid (R.T.)								
–	2984 sh	3143	6	82	3144	4	71	ν_a SCH_3
–	–	3139	1	46	3140	3	54	ν_a SCH_3
2966 s	2968 sh	3093	52	22	3094	42	17	ν_a CH_2
–	–	3089	36	104	3091	43	78	ν_a CH_2
–	–	3075	1	3	3073	4	34	ν_a $CH_3(CH_2)$
–	–	3061	2	123	3063	3	110	ν_a $CH_3(CH_2)$
–	2948 sh	3048	29	175	3049	28	170	ν_s SCH_3
2932 s	2934 (100)	3033	28	13	3036	30	220	ν_s CH_2
2932 s	2934 (100)	3023	0.50	225	3024	14	194	ν_s CH_2
2840 sh	2915 (43)	3021	29	148	3022	20	27	ν_s $CH_3(CH_2)$
1693 s, br	1693 (14)	1760	258	9	1761	244	8	ν C=O
1463 sh	–	1509	10	1	1506	9	4	δ_a $CH_3(CH_2)$
1458 w	–	1499	8	8	1502	8	4	δ_a $CH_3(CH_2)$
1451 sh	1452 (16)	1495	1	12	1487	6	11	δ CH_2
1425 w	1430 (12)	1481	10	11	1484	8	9	δ_a SCH_3
–	1422 sh	1479	6	9	1475	8	10	
1417 w	–	1473	6	11	1463	11	9	δ $CH_2(CO)$
1381 w	–	1414	2	0.2	1417	6	.01	δ_s $CH_3(CH_2)$
1346 w	–	1379	13	3	1379	10	4	ω CH_2
1311 w	–	1346	8	1	1369	1	1	δ_s SCH_3
1278 w	–				1346	10	1	ω CH_2
1259 w	–	1332	4	7				
1221 w	–	1304	10	2	1290	8	3	tω CH_2
1221 w	–	1251	2	1	1240	0.5	6	
1138 s	–	1139	56	4	1134	38	4	ρ $CH_3(CH_2)$
1116 s	1116 (15)	1104	4	16				ρ $CH_3(CH_2)$
1093 sh	1093(10)				1085	9	1	
1050 w	1053 (12)				1058	23	5	ν_a C–C–CH_3
1040 w	1043 (15)	1043	20	5				
1014 vs	–	1019	146	3				ν C–C(O)
999 vs	–				1003	123	3	
–	–	988	1	2	986	7	3	ρ SCH_3
964 sh	–	982	0.2	5	978	22	4	ρ SCH_3
887 m	888 (12)	896	9	4	893	7	4	ρ CH_2
887 m	888 (12)	884	3	6				
861 m	865 (10)				864	15	5	ν_s C–C–CH_3
801 m	803 (6)				807	32	12	ρ CH_2
763 m	766 (6)	758	26	1				
740 sh		736	32	2				ν S–CH_2
–	725 (34)				710	6	7	
–	699 (20)	703	4	14	697	15	14	ν C(O)–S
600 m	604 (15)	575	24	8				$\rho_{out\ of\ plane}$ C=O
580 sh	578 sh				544	14	4	
503 vw	503 (15)	502	3	5				$\rho_{in\ plane}$ C=O
–	494 sh				490	1	4	
–	339 (11)	377	3	1	391	6	1	δ C–C–CH_3
–	309 (21)	291	2	5	330	3	7	δ C–C(O)–C
–	255 (15)	250	11	1	292	0.5	0.7	τ CH_3
–	–	240	1	1	235	2.2	2.6	δ C–C–C(O)
–	–	195	0.5	1.0	179	0.6	0.78	τ C–C(CH_3)
–	–	102	0.3	0.01	130	0.26	0.02	τ C–C(O)
–	–	80	0.05	0.1	81	0.3	1.0	τ SCH_3
–	–	65	0.01	0.5	37	0.2	0.3	τ C–S
–	–	22	0.02	0.1	24	0.3	0.5	τ structural

[a] sh, shoulder; s, strong; w, weak; m, medium; v, very.
[b] Relative band heights in parentheses.
[c] Calculated at B3LYP/6-311++G(d,p) level. Frequencies in cm^{-1} and IR intensity in km mol^{-1}.
[d] ν: stretching, δ: in-plane deformation, γ: out-of-plane deformation, ρ: rocking, ω: wagging, $\tau\omega$: twisting, τ: torsion modes.

bending mode. The bands located at 1381 and 1311 cm^{-1} in the IR spectrum are assigned to the symmetric bending mode of the $CH_3(CH_2)$ and $CH_3(S)$, respectively. The bands corresponding to the $CH_3(CH_2)$ rocking mode appear split in the IR and Raman spectra (See Table 6) indicating the presence of the two conformations mentioned above.

The strong band located at 2966 cm^{-1} in the IR spectrum (2968 cm^{-1} in Raman) is assigned to the CH_2 anti-symmetric stretching mode. The most intense band located at 2934 cm^{-1} in the Raman spectrum (2932 cm^{-1} in IR) is assigned to the CH_2 symmetric stretching mode.

The shoulder located at 1451 cm^{-1} in the IR spectrum (1452 cm^{-1} in Raman) is assigned to the CH_2 bending mode. The bands corresponding to the CH_2 wagging mode appear at 1346, 1278 and 1259 cm^{-1} in the IR spectrum. These bands appear split indicating the presence of the two most stable conformers of the title compound. The experimental IR spectrum between 1550 and 500 cm^{-1} and the corresponding simulated IR of the *gauche–*

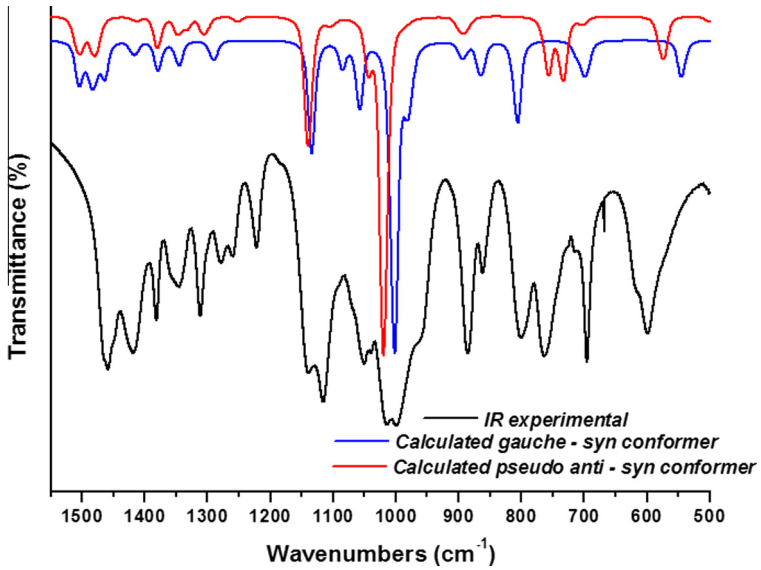

Fig. 7. Experimental and calculated IR spectra (between 1550 and 500 cm^{-1}) for the *gauche–syn* and *pseudo anti–syn* conformers of $CH_3CH_2CH_2C(O)SCH_3$.

syn and *pseudo anti–syn* conformers of the title compound are shown in Fig. 7. The weak band observed at 1221 cm^{-1} in the IR spectrum is assigned to the CH_2 twisting mode and the bands at 887, 801 and 763 cm^{-1} are assigned to the CH_2 rocking mode. The bands mentioned above appear split in the IR spectrum indicating that these bands are important to identify the conformations present in the liquid substance.

Carbonyl group modes. The very strong band located at 1693 cm^{-1} in the IR spectrum is assigned to the C=O stretching mode. The band corresponding to the same mode of vibration appears in the Raman spectrum as a weak band located at 1693 cm^{-1}. These bands are in agreement with the values predicted by calculations performed at B3LYP/6-311++G(d,p) level. The wavenumbers predicted by calculations were 1760 and 1761 cm^{-1} for the *pseudo anti–syn* and *gauche–syn* conformers, respectively.

The bands observed at 600 and 580 cm^{-1} in the IR spectrum (604 and 578 cm^{-1} in Raman) are assigned to the C=O out-of-plane bending mode. The band corresponding to the mode mentioned above appears split showing the presence of the two conformations (See Fig. 7 and Table 6). The very weak band located at 503 cm^{-1} in the IR spectrum is assigned to the C=O in-plane bending mode. The Raman spectrum shows two bands at 503 and 494 cm^{-1} corresponding to the mode mentioned above.

Skeletal modes. The band corresponding to the C–C–CH_3 anti-symmetric stretching mode appears split into two components at 1050 and 1040 cm^{-1} in the IR spectrum (1053 and 1043 cm^{-1} in Raman) indicating the presence of the two conformers. This assignment is in agreement with the calculated values 1058 and 1043 cm^{-1} for *gauche–syn* and *pseudo anti–syn* conformers, respectively. The bands located at 887 and 861 cm^{-1} in the IR spectrum (888 and 865 cm^{-1} in Raman) are assigned to the C–C–CH_3 symmetric stretching mode of *pseudo anti–syn* and *gauche–syn* conformers, respectively. This assignment is in agreement with the values calculated for both conformers (884 and 864 cm^{-1}). The IR spectrum shows a shoulder located at 740 cm^{-1} and the Raman spectrum shows a band located at 725 cm^{-1}. These bands are assigned to the S-CH_2 stretching mode for *pseudo anti–syn* and *gauche–syn* conformers, respectively. The band located at 699 cm^{-1} in the Raman spectrum is assigned to the C(O)–S stretching mode.

The bands located at 339 and 309 cm^{-1} in the Raman spectrum are assigned to the C–C–CH_3 and C–C(O)–C bending modes, respectively.

Torsional modes. The band located at 255 cm^{-1} in the Raman spectrum is assigned to the CH_3 torsional mode. The bands corresponding to the other torsional modes have not been observed in the Raman spectrum of the liquid substance.

Conclusions

The optimized molecular geometries and the conformational analysis for S-methyl thiobutanoate compound, $CH_3CH_2CH_2C(O)SCH_3$ have been calculated using MP2 and DFT methods (B3LYP and mPW1PW91) and different basis sets. The structural results indicate that the *pseudo anti–syn* conformation is the most stable form. The geometrical parameters of the title compound calculated are in good agreement with the values reported for related molecules by means of GED measurements.

The NBO analysis was performed to justify the preferred conformation of the title compound. The hyper-conjugative interactions are more favored in the *pseudo anti–syn* conformer than in the others. The analysis performed by means of the AIM indicates that the intramolecular hydrogen interaction O(2)···H(7) is very weak and the C(1)–S(3) ellipticity value shows that the electrons of this bond are not delocalized.

HOMO–LUMO calculations have been performed for the title compound. The energy gap between the HOMO and LUMO molecular orbital is predicted to be 6.232 eV, a relatively high value that shows high molecular chemical stability and low reactivity. Fukui functions, local softness and electrophilicity indices were calculated in order to determine local reactive sites for the molecular system during electrophilic, nucleophilic and radical attacks. According to $f^{\pm}$, $S^{\pm}$ and $\omega^{\pm}$ values, the C(1) site is the most favorable for nucleophilic attack. The most favorable site for electrophilic and radical attacks is *S*(3).

The analysis of the IR and Raman spectra of the title compound in liquid phase agrees with the presence of *pseudo anti–syn* and *gauche–syn* conformers by resolution of some normal modes of vibration.

Please cite this article in press as: D.M. Gil et al., Vibrational studies (FTIR and Raman), conformational analysis, NBO, HOMO–LUMO and reactivity descriptors of S-methyl thiobutanoate, $CH_3CH_2CH_2C(O)SCH_3$, Spectrochimica Acta Part A: Molecular and Biomolecular Spectroscopy (2015), http://dx.doi.org/10.1016/j.saa.2015.04.097

Uncited reference

Q3 [27].

Appendix A. Supplementary data

Supplementary data associated with this article can be found, in the online version, at http://dx.doi.org/10.1016/j.saa.2015.04.097.

References

[1] C. Deduve, Am. Sci. 83 (1995) 428.
[2] A. Lehninger, D.L. Nelson, M.M. Cox, Princ. Biochem., Fourth ed., Omega, Spain, 2005.
[3] A.M. Sourabié, H.E. Spinnler, Bourdat-Dechamps, M.R. Tallon, S. Landaud, P. Bonnarme, Appl. Microbiol. Biotechnol. 93 (2012) 1673.
[4] C.O. Della Védova, R.M. Romano, H. Oberhammer, in: J. Org. Chem. 69 (2004) 5395.
[5] A.M.M. El-Aasar, C.P. Nash, L.L. Ingraham, Biochemistry 21 (1982) 1972.
[6] G.L. Jones, D.G. Lister, N.L. Owen, M.C.L. Gerry, P.J. Palmieri, Mol. Spectrosc. 60 (1976) 34.
[7] M.F. Erben, R. Boese, Védova C. Della, O. Oberhammer, H. Willner, J. Org. Chem. 71 (2006) 616.
[8] M.E. Defonsi Lestard, M.E. Tuttolomondo, E.L. Varetti, D.A. Wann, H.E. Robertson, D.W.H. Rankin, A. Ben Altabef, in: J. Raman Spectrosc. 40 (2009) 2053.
[9] M.E. Defonsi Lestard, M.E. Tuttolomondo, D.A. Wann, H.E. Robertson, D.W.H. Rankin, A. Ben Altabef, J. Raman Spectrosc. 41 (2010) 1357.
[10] M.E. Defonsi Lestard, M.E. Tuttolomondo, E.L. Varetti, D.A. Wann, H.E. Robertson, D.W.H. Rankin, A. Ben Altabef, J. Mol. Struct. 917 (2009) 183.
[11] M.E. Defonsi Lestard, M.E. Tuttolomondo, D.A. Wann, H.E. Robertson, D.W.H. Rankin, A. Ben Altabef, J. Chem. Phys. 131 (2009) 214303.
[12] Frisch M.J., Pople J.A., Binkley J.S., J. Chem. Phys. 80 (1984) 3265. Frisch, M.J.; Trucks, G.W.; Schlegel, H.B.; Scuseria, G.E.; Robb, M.A.; Cheeseman, J.R.; Montgomery, Jr., J.A.; Vreven, T.; Kudin, K.N.; Burant, J.C.; Millam, J.M.; Iyengar, S.S.; Tomasi, J.; Barone, V.; Mennucci, B.; Cossi, M.; Scalmani, G.; Rega, N.; Petersson, G.A.; Nakatsuji, H.; Hada, M.; Ehara, M.; Toyota, K.; Fukuda, R.; Hasegawa, J.; Ishida, M.; Nakajima, T.; Honda, Y.; Kitao, O.; Nakai, H.; Klene, M.; Li, X.; Knox, J.E.; Hratchian, H.P.; Cross, J.B.; Bakken, V.; Adamo, C.; Jaramillo, J.; Gomperts, R.; Stratmann, R.E.; Yazyev, O.; Austin, A.J.; Cammi, R.; Pomelli, C.; Ochterski, J.W.; Ayala, P.Y.; Morokuma, K.; Voth, G.A.; Salvador, P.; Dannenberg, J.J.; Zakrzewski, V.G.; Dapprich, S.; Daniels, A.D.; Strain, M.C.; Farkas, O.; Malick, D.K.; Rabuck, A.D.; Raghavachari, K.; Foresman, J.B.; Ortiz, J.V.; Cui, Q.; Baboul, A.G.; Clifford, S.; Cioslowski, J.; Stefanov, B.B.; Liu, G.; Liashenko, A.; Piskorz, P.; Komaromi, I.; Martin, R.L.; Fox, D.J.; Keith, T.; Al-Laham, M.A.; Peng, C.Y.; Nanayakkara, A.; Challacombe, M.; Gill, P.M.W.; Johnson, B.; Chen, W.; Wong, M.W.; Gonzalez, C.; Pople, J.A.; Gaussian 03, Revision C.01. Gaussian Inc, Wallingford CT (2004).
[13] C. Møller, M.S. Plesset, Phys. Rev. 46 (1934) 618.
[14] R. Krishnan, J.S. Binkley, R. Seeger, J.A. Pople, J. Chem. Phys. 72 (1980) 650.
[15] A.D. McLean, G.S. Chandler, J. Chem. Phys. 72 (1980) 5639.
[16] M.J. Frisch, J.A. Pople, J.S. Binkley, J. Chem. Phys. 80 (1984) 3265.
[17] W.J. Hehre, P.V.R. Schleyer, J.A. Pople, Ab initio Molecular Orbital Theory, Wiley, New York, 1986.
[18] A.D. Becke, J. Chem. Phys. 98 (1993) 5648.
[19] C. Lee, W. Yang, R.G. Parr, Phys. Rev. B 37 (1988) 785.
[20] C. Alamo, B. Barone, J. Chem. Phys. 108 (1998) 664.
[21] E.D. Glendening, J.K. Badenhoop, A.D. Reed, J.E. Carpenter, F.F. Weinhold, Theoretical Chemistry Institute, University of Wisconsin, Madison, WI, 1996.
[22] R.F.W. Bader, Atoms in Molecules, A quantum Theory, Clarendon Press, Oxford, 1990.
[23] F. Biegler-Köning, J. Schönnbohn, D.J. Bayles, Comput. Chem. 22 (2001) 545.
[24] V. Krishnakumar, G. Keresztury, T. Sundius, R.J. Ramanamy, Mol. Struct. 702 (2004) 9.
[25] M.E. Tuttolomondo, A. Navarro, T.P. Ruiz, E.L. Varetti, S.A. Hayes, D.A. Wann, H.E. Robertson, D.W.H. Rankin, A. Ben Altabef, J. Phys. Chem. A 111 (2007) 9952.
[26] D.M. Gil, M.E. Tuttolomondo, A. Ben Altabef, J. Spectrochim. Acta A 123 (2014) 290.
[27] U. Koch, P.L.A. Popelier, J. Phys. Chem. 99 (1995) 9747.
[28] W. Koch, G. Frenking, J. Gauss, D. Cremer, J.R. Collins, J. Am. Chem. Soc. 109 (1987) 5917.
[29] I. Rozas, I. Alkorta, J. Elguero, J. Am. Chem. Soc. 122 (2000) 11154.
[30] V. Arjuan, M. Kalaivani, S. Senthikumari, S. Mohan, J. Spectrochim. Acta A 115 (2013) 154.
[31] J. Sponer, P. Hobza, Int. J. Quantum Chem. 57 (1996) 959.
[32] M. Karabacak, L. Sinha, O. Prasad, Z. Cinar, M.J. Cinar, Spectrochim. Acta A 93 (2012) 33.
[33] S.K. Pathak, R. Srivastava, K.A. Sachan, O. Prasad, L. Sinha, A.M. Asiri, M. Karabacak, J. Spectrochim. Acta A 135 (2015) 283.
[34] R.G. Parr, R.G. Pearson, J. Am. Chem. Soc. 105 (1983) 7512.
[35] R.G. Parr, W.J. Yang, J. Am. Chem. Soc. 106 (1984) 4048.
[36] E. Chamorro, P. Pérez, J. Chem. Phys. 123 (2005) 14107.
[37] J. Padmanabhan, R. Parthasarathi, V. Subramanian, P. Chattaraj, J. Phys. Chem. A 111 (2007) 1358.
[38] S.E. Ulic, E.M. Coyanis, R.M. Romano, C.O. Della Védova, J. Spectrochim. Acta A 54 (1998) 695.
[39] M.E. Defonsi Lestard, M.E. Tuttolomondo, A. Ben Altabef, in: J. Spectrochim. Acta A 135 (2015) 907.

Please cite this article in press as: D.M. Gil et al., Vibrational studies (FTIR and Raman), conformational analysis, NBO, HOMO–LUMO and reactivity descriptors of S-methyl thiobutanoate, $CH_3CH_2CH_2C(O)SCH_3$, Spectrochimica Acta Part A: Molecular and Biomolecular Spectroscopy (2015), http://dx.doi.org/10.1016/j.saa.2015.04.097